D2.2(HIRS): Report on the HIRS FCDR: Uncertainty

Gerrit Holl (1), Emma Woolliams (2), Jonathan Mittaz(1,2)

(1) University of Reading, (2) National Physical Laboratory

31st August 2019

Contents

1 Introduction

1.1 Scope

This document is one of the five documents that make up the D2-2 report on "traceability chains for FCDRs". Since the original project proposal our thoughts have refined and while this document describes the "sequence of measurement standards and calibrations that is used to relate a measurement result to a reference" (the VIM definition of a traceability chain), it is not presenting this in the form of a chain.

This document provides an overview of the uncertainty analysis for the analysed sensors along with the methods to establish metrological traceability for the developed FCDRs.

This document is specifically about the HIRS FCDR. The document D2-2a provides an overview of the purposes of these documents and explains the basis of the effects tables.

1.2 Version Control

Version	Reason	Reviewer	Date of Issue
1.a			
1.b			
1.c			

1.3 Applicable and Reference Documents

1.3.1 D2-2 set of documents

D2-2a	Principles behind the FCDR effects table
D2-2(microwave)	Report on the MW FCDR: Uncertainty
D2-2(HIRS)	Report on the HIRS FCDR: Uncertainty (This document)
D2-2(AVHRR)	Report on the AVHRR FCDR: Uncertainty
D2-2(MVIRI)	Report on the MVIRI FCDR: Uncertainty

1.3.2 References

Cao, C., K. Jarva and P. Ciren (2007). "An Improved Algorithm for the Operational Calibration of the High-Resolution Infrared Radiation Sounder". In: J. Atmos. Oceanic Technol. 24.2, pp. 169–181. doi: 10.1175/JTECH2037.1.

Chen, R., C. Cao and W. P. Menzel (2013). "Intersatellite calibration of NOAA HIRS CO_2 channels for climate studies". In: J. Geophys. Res. 118.11, pp. 5190–5203. doi: 10.1002/jgrd.50447.

Weinreb, H. P., H. E. Fleming, L. M. McMillin and A. C. Neundorffer (1981). Transmittances for the TIROS Operational Vertical Sounder. Tech. rep. NESS 85. Washington D.C.

Robel, J., A. Graumann, K. Kidwell, R. Aleman, G. Goodrum, T. Mo, I. Ruff, J. Askew, A. Graumann, B. Muckle, J. Sapper, D. Bowman, P. Green, S. Patterson, J. Sullivan, S. Brown, E. Harrod, N. Peterski, J. Throwe, E. Brown, M. Hollinger, W. Planet, D. Wark, W. Clouse, J. Knoll, B. Ramsay, M. Weinreb, D. Fineberg, S. Krimchansky, N. Rao, W. Winston, L. Flynn, L. McMillin, G. Robinson, T. Wrublewski, H. Goldberg, T. Miller, D. Ross and T. Kleespies (2014). NOAA KLM User's Guide with NOAA-N, -N' Supplement. Tech. rep. National Oceanic and

Atmospheric Administration, National Environmental Satellite, Data, and Information Service, National Climatic Data Center, Remote Sensing and Applications Division.

T. Chang and C. Cao. "Modeling Infrared Radiometer Self-Emission With Application to MetOp/HIRS". In: IEEE T. Geosci. Remote 52.6 (2014), pp. 3141–3149. doi: 10.1109/TGRS.2013.2270953.

1.4 Glossary

BT	Brightness Temperature
EUMETSAT	European Organisation for the Exploitation of Meteorological Satellites
FCDR	Fundamental Climate Data Record
FOV	Field Of View
HIRS	High-resolution Infrared Radiation Sounder
IASI	Infrared Atmospheric Sounding Interferometer
ICCT	Internal Cold Calibration Target
IWCT	Internal Warm Calibration Target
NCC	National Calibration Center
NESDIS	National Environmental Satellite, Data, and Information Service
NOAA	National Oceanic and Atmospheric Administration
PRT	Platinum Resistance Thermometer
SNO	Simultaneous Nadir Observation
SRF	Spectral Response Function
STAR	Center for Satellite Applications and Research
TIROS	Television Infra-Red Observation Satellite

2 FIDUCEO effects tables

In FIDUCEO we have defined an effects table which describes

- the uncertainty associated with a given effect
- the sensitivity coefficient required to propagate uncertainties associated with that effect to uncertainties associated with the measurand (Earth radiance, reflectance or brightness temperature)
- the correlation structure over spatial, temporal and spectral scales for errors from this effect

The concepts behind the effects tables are described in D2-2a. In this document we provide a discussion of the effects tables and uncertainty propagation for a single instrument series; here the HIRS FCDR.

3 The HIRS instrument

HIRS is a space-borne radiometer measuring radiation emitted and reflected by the Earth surface and atmosphere. HIRS measures radiation in 20 channels: 12 terrestrial (thermal) infrared, 7 shortwave infrared, and 1 visible. The first version of HIRS was launched in 1975 on Nimbus-6, then with 17 channels. The first operational HIRS, and the earliest one we will consider in this study, is the 20-channel HIRS/2, launched in 1978 on TIROS-N. Since then, there have been 10 instances of HIRS/2 (one of which failed to reach orbit), 3 instances of HIRS/3, and 4 instances of HIRS/4 (see Table 1). Differences between subsequent versions of HIRS include a smaller sensor footprint, adjustment of channel positions, and more rigorous pre-launch characterisation.

Table 1 A summary of the coverage of the different HIRS instruments

Generation	Satellite	Start	End
HIRS/1	NIMBUS-6	1975-08-17	1976-03-04
HIRS/2	TIROS-N	1978-10-29	1980-01-30
HIRS/2	NOAA-6/A	1979-06-30	1983-03-05
HIRS/2	NOAA-7/C	1981-08-24	1984-12-31
HIRS/2	NOAA-8/E	1983-05-03	1985-10-14
HIRS/2	NOAA-9/F	1985-02-25	1988-11-07
HIRS/2	NOAA-10/G	1986-11-25	1991-09-16
HIRS/2I	NOAA-11/H	1988-11-08	1998-12-31
HIRS/2	NOAA-12/D	1991-09-16	1998-12-14
-	NOAA-13	Launch failure	
HIRS/2I	NOAA-14/J	1995-01-01	2006-10-10
HIRS/3	NOAA-15/K	1999-01-01	
HIRS/3	NOAA-16/L	2001-01-01	2014-06-05
HIRS/3	NOAA-17/M	2002-07-10	2013-04-09
HIRS/4	NOAA-18/N	2005-06-05	
HIRS/4	NOAA-19/N'	2009-04-01	
HIRS/4	MetOp-A	2006-11-21	
HIRS/4	MetOp-B	2013-01-15	

Table 2 shows the positions for the thermal HIRS channels on all satellites, according to their measured SRFs, where the position is defined by the SRF centroid wavelength, $\lambda_{ch,c}$ is the centroid wavelength for channel ch, calculated as the SRF-weighted mean wavelength,

$$\lambda_{ch,c} = \int \lambda \xi_{ch}(\lambda)\,\mathrm{d}\lambda \qquad \text{Eq 3-1}$$

where $\xi_{ch}(\lambda)$ is the normalised spectral response function for that channel, and λ is wavelength.

Table 2 Centroid wavelength for the HIRS channels

Channel	Wavelength [μm]	Detector	Notes
1	14.95	HgCdTe	
2	14.70		
3	14.47		
4	14.21		
5	13.95		
6	13.65		
7	13.34		
8	11.11		
9	9.71		
10	8.2 / 12.47		HIRS-2 / rest
11	7.33		
12	6.7 / 6.52		HIRS-2+2I / rest
13	4.57	InSb	
14	4.52		
15	4.67		
16	4.42		
17	4.18		
18	3.97		
19	3.76	Si	

HIRS-carrying satellites fly in sun-synchronous orbits with equator crossing times at launch that are either mid-morning or mid-afternoon. HIRS scans the Earth perpendicular to the direction of flight in 56 observations at angles in a range of ±49.5°, which results in a swath width of 1089.4 km from nadir to the centre of the outermost Field of View (FOV). HIRS footprints have an Instantaneous Field of View (FOV) diameter of 20.4 km for HIRS/2/2I/3 and 10.2 km for HIRS/4.

As HIRS is a thermal infrared instrument, its gain depends on self-emission and therefore varies as the instrument's temperature changes. This is dealt with through an on-board calibration cycle. Within each calibration cycle, HIRS observes Earth for 38 (for HIRS/3 and HIRS/4) or 37 (for HIRS/2) scanlines, then makes 48 useable observations of deep space and 48 of the Internal Warm Calibration Target (IWCT)[1]. HIRS/2 additionally makes observations of an Internal Cold Calibration Target (ICCT). The space and IWCT measurements are used to determine the gain and offset that are valid for the 38 Earth scanlines in the calibration cycle. For the operational HIRS calibration by NOAA[2], these measurements determine the slope and offset of a quadratic calibration, with the non-linear term determined before launch, although in practice this term is set to zero. The precise way in which the slope and offset are interpolated and smoothed between calibration cycles for existing operational HIRS varies between calibration versions, described in detail by Cao, Jarva and Ciren (2007)[3].

HIRS radiances are calibrated in units of mW m^{-2} sr^{-1} cm. The calibration assumes the IWCT is a grey body. Earth view radiances are usually converted to Brightness Temperatures (BTs) in units of kelvin. While monochromatic radiances can be converted to BTs by inverting the Planck function, a channel-integrated radiance cannot be explicitly inverted.. There are different ways around this. The established approach, such as applied by NOAA and EUMETSAT, is to calculate "band correction factors" following Weinreb et al. (1981), that need to be applied upon the conversion to brightness temperatures. Those factors are calculated by calculating $L_{ch}(T_{\mathrm{b}})$ for channel ch,

$$L_{ch}(T_{\mathrm{b}}) = \int \xi_{ch}(\lambda) L_{\mathrm{BB}}(\lambda, T_{\mathrm{b}}) \mathrm{d}\lambda$$

<div align="right">*Eq 3-2*</div>

Where L_{ch} is the radiance for channel ch, $\xi_{ch}(\lambda)$ is the normalised spectral response function, $L_{\mathrm{BB}}(\lambda, T_{\mathrm{b}})$ is the radiance of a blackbody at the brightness temperature T_{b} given by the Planck function and λ is wavelength[4]. Using Eq 3-2, it is straightforward to construct a lookup table to calculate the brightness temperature as a function of radiance. The lookup table can either be used directly, or can be used to calculate a set of band correction factors.

3.1 The HIRS measurement function

The HIRS FCDR is built on the measurement function which calculates the Earth Radiance L_{E} from the Earth Count C_{E}. A correction is made for the instrument self-emission radiance in Earth view, $L_{\mathrm{self,E}}$, which is a

---

[1] In principle it observes each 56 times, but the first 8 views are very often contaminated by the spacecraft while the mirror is still swinging to the right position, so in practice only 48 views are useable most of the time (sometimes less, but that is a separate problem).

[2] National Oceanic and Atmospheric Administration

[3] Note that there are three different operational calibration methods used by NOAA and one by EUMETSAT (European Organisation for the Exploitation of Meteorological Satellites). Here we adapt the Cao, Jarva and Ciren calibration.

[4] Or alternatively, using the frequency or wavenumber versions of Planck's law this can be adjusted for other base units

function of the instrument temperature, T_{inst} and an offset correction is determined from the averaged space view counts during the calibration cycle, $\bar{C}_{\text{S}}$. T_{inst} is estimated for every scanline. The measurement function is

$$L_{\text{E}} = \alpha\left(C_{\text{E}} - \bar{C}_{\text{S}}\right) + a_1\left(C_{\text{E}}^2 - \bar{C}_{\text{S}}^2\right) - \left(L_{\text{self,E}}\left(T_{\text{inst}}\right) - L_{\text{self,S}}\left(T_{\text{inst}}\right)\right) + a_3 + 0.$$

<div align="right">Eq 3-3</div>

The 0 term represents the assumption that this form of the equation is valid and, for example, that there are no higher order nonlinearities. The nonlinearity coefficient a_1 and offset a_3 are coefficients to be determined during harmonisation to a reference sensor.

The gain term is determined from the calibration cycle measurements of the IWCT and space views, as

$$\alpha = -\frac{\tilde{L}_{\text{IWCT}} + L_{\text{self,IWCT}}\left(T_{\text{inst}}\right) - L_{\text{self,S}}\left(T_{\text{inst}}\right) - a_1\left(\bar{C}_{\text{IWCT}}^2 - \bar{C}_{\text{S}}^2\right)}{\bar{C}_{\text{IWCT}} - \bar{C}_{\text{S}}}.$$

<div align="right">Eq 3-4</div>

where, $\tilde{L}_{\text{IWCT}}$ is the band-integrated IWCT radiance, $L_{\text{self,IWCT}}$ is the self-emission radiance when viewing the IWCT, $L_{\text{self,S}}\left(T_{\text{inst}}\right)$ is the self-emission radiance when viewing space and $\bar{C}_{\text{IWCT}}, \bar{C}_{\text{S}}$ are the measured counts when viewing the IWCT and space respectively, averaged over the different individual measurements in the calibration cycle.

The band-integrated IWCT radiance is conceptually[5] given by

$$\tilde{L}_{\text{IWCT}} = \int\left(\left(\varepsilon_{ch} + a_2\right)L_{\text{BB}}\left(\lambda, T_{\text{IWCT}}\right) + \left(1 - \varepsilon_{ch} - a_2\right)L_{\text{refl}}\left(\lambda\right)\right)\xi_{ch}\left(\lambda\right)\mathrm{d}\lambda + 0.$$

<div align="right">Eq 3-5</div>

where, $\varepsilon\left(\lambda_{ch,\text{c}}, T_{\text{IWCT}}\right)$ is the emissivity of the IWCT (stated by Wang, Cao, and Ciren (2007) to be 0.98), a_2 is a correction to this tabulated emissivity that is determined through harmonisation and $\xi_{ch}\left(\lambda\right)$ is the normalised spectral response function. Although physically, ε may be expected to change as a function of temperature or wavelength, we assume constant emissivity within each channel; any deviation should be encompassed in the uncertainty associated with a_2, which can differ per channel. The IWCT radiance is given by Planck's law,

$$L_{\text{BB}}\left(\lambda, T_{\text{IWCT}}\right) = c_{1,L}\Big/\left(\lambda^5\left(\exp\left[c_2 / \lambda T_{\text{IWCT}}\right] - 1\right)\right),$$

<div align="right">Eq 3-6</div>

Where $c_{1,L} = 2hc^2$ is the first radiation constant for radiance, and $c_2 = hc/k_{\text{B}}$ is the second radiation constant. The term L_{refl} is the radiance reflected by the IWCT from other sources, which needs to be modelled with the details yet to be determined (this may be part of the harmonisation); in the present version it is set to zero. In practice this integral is calculated from discrete values of the spectral response function using the trapezium rule. The +0 term represents the extent to which that calculation does not represent the true band-integrated radiance, for example due to the numerical determination of the integral.

As a temporary measure in the present version, the band-integrated IWCT radiance is approximated using band coefficients, to ease the propagation of uncertainties:

---

[5] At present the band-integrated IWCT radiance is calculated according to Eq 3-7, see below.

$$\tilde{L}_{\text{IWCT}} = \left(\varepsilon_{ch} + a_2\right) L_{\text{BB}}\left(\lambda_{\text{eff},ch}, c_{\text{a},ch} + c_{\text{b},ch} T_{\text{IWCT}}\right) + \left(1 - \varepsilon_{ch} - a_2\right) L_{\text{refl}}\left(\lambda_{\text{eff},ch}\right)$$

<div align="right">*Eq 3-7*</div>

where the temperature corrections, $c_{\text{a},ch}, c_{\text{b},ch}$ and effective wavelength, $\lambda_{\text{eff},ch}$ are determined from the SRF by a fitting process.

The temperature of the IWCT is calculated from a simple mean of the temperatures obtained from N platinum resistance thermometers (PRTs) mounted on the IWCT. N is 4 for HIRS/2 and HIRS/3, and N is 5 for HIRS/4. The PRTs measure a count which is converted to temperature using a calibration equation expressed as a fifth order polynomial. The calibration coefficients for the PRTs were determined prelaunch through comparison with a more accurate thermometer at different temperatures.

The self-emission radiances given in Eq 3-3, Eq 3-2 and Eq 3-4 for the Earth, Space and IWCT views ($v =$ E,S,IWCT respectively) are in principle determined by

$$L_{\text{self},v}\left(T_{\text{inst}}\right) = \sum_i \left[\Omega_{v,i} \int \xi_{ch}\left(\lambda\right) \varepsilon_i\left(\lambda_{ch,\text{c}}, T_i\right) L_{\text{BB}}\left(\lambda, T_i\right) \text{d}\lambda\right] + 0 \ .$$

<div align="right">*Eq 3-8*</div>

where the sum is performed over different [...] components i, which have a field of view $\Omega_{v,i}$ in that view and an emissivity at the channel wavelength of $\varepsilon_i\left(\lambda_{ch,\text{c}}, T_i\right)$ and a temperature T_i and are treated as grey-bodies, using the Planck equation multiplied by an emissivity. However, in practice we have insufficient information to determine all the view factors, and not all components in the field of view have their temperatures measured. In practice, the self-emission is currently estimated with:

$$L_{\text{self},y} = \sum_i k_i T_i^4 + 0 \ .$$

<div align="right">*Eq 3-9*</div>

where i refers to different temperatures, currently the baseplate, internal warm calibration target, scanmirror, scanmotor, and secondary telescope. The coefficients are trained using linear regression in a moving 24-hour window and updated every 6 hours.

The $+0$ term accounts for the assumptions implicit in this simplified model.

3.2   Measurement Function Diagram

Figure 1 illustrates the measurement function diagram for HIRS, with the sources of uncertainty at the end. Note that both the contents and the visualisation are still preliminary and may change as we find more optimal ways of implementing the FCDR.
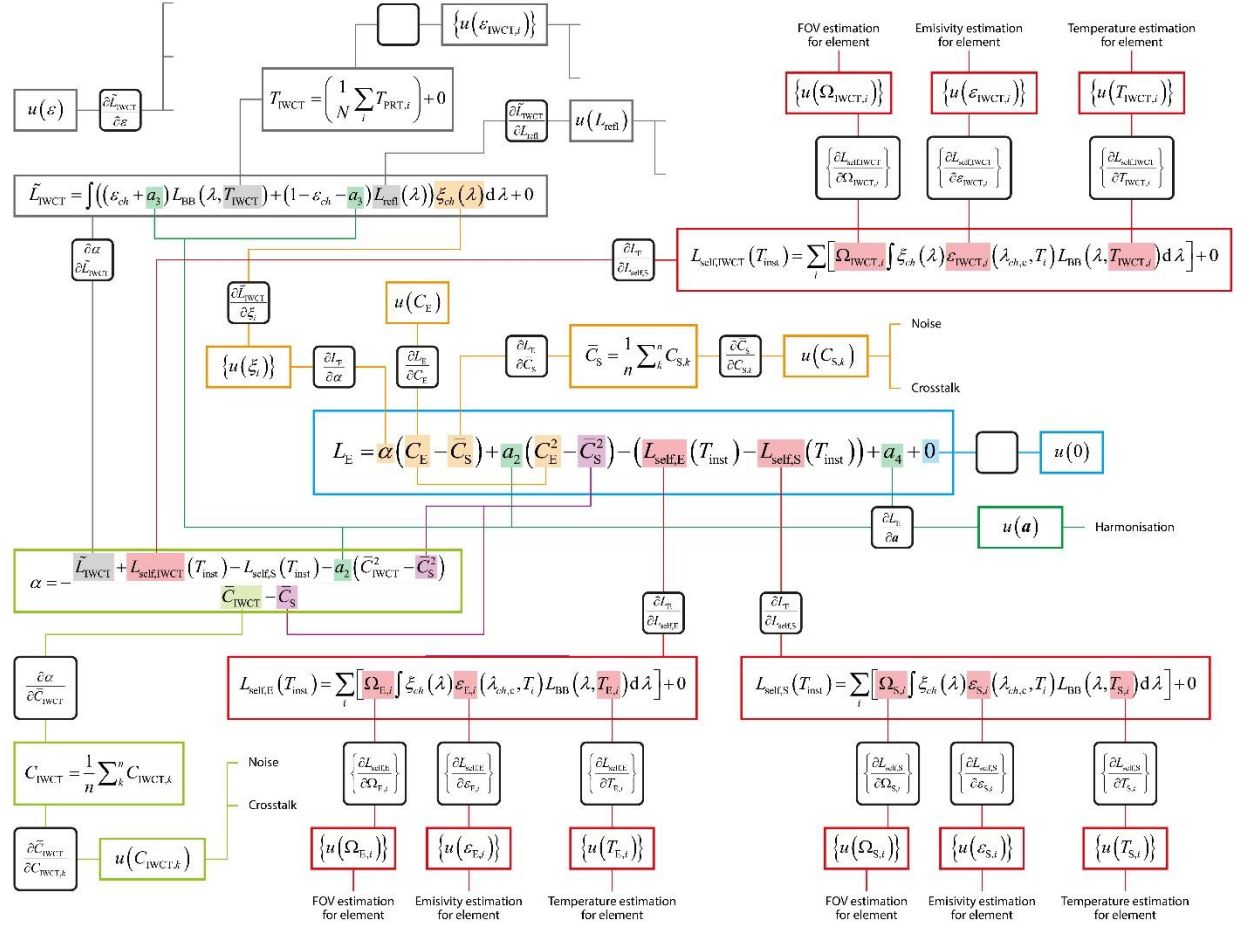
Figure 1: illustration of HIRS measurement function diagram, preliminary version.

4   A discussion of different terms

In this section we consider the different sources of uncertainty and discuss the error correlation structure for this effect in the different dimensions using the Effects Tables that have been described in D2-2a. A full description of how this effect was evaluated is beyond the scope of this paper, but references are given, or details are provided in the appendices.

4.1   Noise in Earth Counts, Averaged Space Counts and Averaged IWCT Counts

Each detector measurement (a count) is sensitive to noise and channel cross-talk. At present we do not have sufficient information to separate these two effects. The noise in the averaged space counts and averaged IWCT counts can be estimated by considering the statistical properties of the 48 individual counts of each of these measured during the calibration cycle, with the uncertainty associated with the mean reduced from the uncertainty associated with a single value. This analysis, described in Appendix A, showed unexpected correlations between channels and over time which is likely to be due to cross-talk. The noise in the Earth count cannot easily be determined statistically due to the rapid variation of the Earth scene. Instead, the Earth count noise is taken as the larger of the Space and IWCT count noises for a particular calibration cycle.

Without crosstalk, the Earth Count error is uncorrelated. That is, the error due to noise in the measured count in one pixel is independent of that in the next pixel because they are separate measurements. Cross-

talk effects make this simplified picture slightly more complex and both positive and negative correlations exist between channels and between views taken closely in time, either for Earth or for calibration views. Some details are included in Appendix A.1 and in a journal publication currently in preparation.

Without crosstalk, the Space and IWCT count noise errors are constant within a calibration cycle (i.e. for all Earth pixels within a 38 scanline window). This is because these values are only calculated once within the calibration cycle. If the gain calculated with Eq 3-4 is smoothed through a rolling average with gains for previous and subsequent calibration cycles, then there will be some error correlation with pixels in previous and subsequent calibration cycles. Overall the correlation coefficient will take the form of a stepped triangle (see D2-2a).

The cross-talk effect complicates this picture further, although the temporal cross-talk correlation is within the timescale of a single calibration cycle, so we can still consider separate calibrations to have independent errors. Cross talk does create correlation between spectral channels for all three counts. This correlation between channels is determined statistically for the IWCT counts and space counts and an estimate is made for space counts based on the statistical results for the other two sources.

Table 3 Effects tables for the Earth, averaged-Space and averaged-IWCT counts

Table descriptor				
Name of effect		Earth Count Noise	Averaged Space Count Noise	Averaged IWCT Count Noise
Affected term in measurement function		C_{E}	$\bar{C}_{\mathrm{S}}$	$\bar{C}_{\mathrm{IWCT}}$
Instruments in the series affected		All	All	All
Correlation type and form	**Pixel-to-pixel [pixels]**	Random*	Rectangular Absolute	Rectangular Absolute
	from scanline to scanline [scanlines]	Random*	Stepped triangle absolute	Stepped triangle absolute
	between images [images]	N/A	N/A	N/A
	Between orbits [orbit]	Random	Random	Random
	Over time [time]	Random	Random	Random
Correlation scale	**Pixel-to-pixel [pixels]**	[0]	$\left[-\infty,+\infty\right]$	$\left[-\infty,+\infty\right]$
	from scanline to scanline [scanlines]	[0]	Provided for each pixel to define the stepped triangle absolute as [-a,b,n] –a: scanlines before this one, b scanlines after this one within calibration window. a+b+1 = 38, n = number of calibration windows	Provided for each pixel to define the stepped triangle absolute, [-a,b,n] a+b+1 = 38, n = number of calibration windows averaged.

			averaged in rolling average.	
	between images [images]	N/A	N/A	N/A
	Between orbits [orbit]	[0]	[0]	[0]
	Over time [time]	[0]	[0]	[0]
Channels/bands	List of channels / bands affected	All	All	All
	Error correlation coefficient matrix	Provide from statistical analysis, **see Appendix**	Provide from statistical analysis, **see Appendix**	Provide from statistical analysis, **see Appendix**
Uncertainty	PDF shape	Digitised Gaussian	Digitised Gaussian	Digitised Gaussian
	units	Counts	Counts	Counts
	magnitude	Provided per scanline	Provided per scanline	Provided per scanline
Sensitivity coefficient		$\dfrac{\partial L_{\mathrm{E}}}{\partial C_{\mathrm{E}}}$, Eq 4-1	$\dfrac{\partial L_{\mathrm{E}}}{\partial \bar{\bar{C}}_{\mathrm{S}}}$, Eq 4-2	$\dfrac{\partial L_{\mathrm{E}}}{\partial \bar{C}_{\mathrm{IWCT}}}$, Eq 4-3

The sensitivity coefficients are

$$\frac{\partial L_{\mathrm{E}}}{\partial C_{\mathrm{E}}} = \alpha + 2a_1 C_{\mathrm{E}} \; . \tag{Eq 4-1}$$

$$\frac{\partial L_{\mathrm{E}}}{\partial \bar{\bar{C}}_{\mathrm{S}}} = \left(C_{\mathrm{E}} - \bar{C}_{\mathrm{S}} \right) \frac{\partial \alpha}{\partial \bar{\bar{C}}_{\mathrm{S}}} - \alpha + 2a_1 \bar{C}_{\mathrm{S}}$$

$$\frac{\partial \alpha}{\partial \bar{C}_{\mathrm{S}}} = \frac{-2a_1 \bar{C}_{\mathrm{S}}}{\bar{C}_{\mathrm{IWCT}} - \bar{C}_{\mathrm{S}}} + \frac{\alpha}{\left(\bar{C}_{\mathrm{IWCT}} - \bar{C}_{\mathrm{S}} \right)} \tag{Eq 4-2}$$

$$\frac{\partial L_{\mathrm{E}}}{\partial \bar{C}_{\mathrm{IWCT}}} = \left(C_{\mathrm{E}} - \bar{C}_{\mathrm{S}} \right) \frac{\partial \alpha}{\partial \bar{C}_{\mathrm{IWCT}}}$$

$$\frac{\partial \alpha}{\partial \bar{C}_{\mathrm{IWCT}}} = \frac{2a_1 \bar{C}_{\mathrm{IWCT}}}{\bar{C}_{\mathrm{IWCT}} - \bar{C}_{\mathrm{S}}} - \frac{\alpha}{\bar{C}_{\mathrm{IWCT}} - \bar{C}_{\mathrm{S}}} \tag{Eq 4-3}$$

4.2 Spectral response function

The spectral response functions of the different channels were determined pre-launch through an experimental characterisation and are defined by measurements at discrete wavelengths. The spectral response function is most significantly used in determining the band-integrated radiance of the IWCT and in

determining the brightness temperature from the measured radiance. It also affects the self-emission terms, but is not currently used explicitly in the model to estimate self-emission.

There are different types of uncertainty that are likely to have affected the original calibration of the spectral response function. In addition, the spectral response function is likely to have changed in orbit due to degradation of optical components, temperature sensitivities of the filters and any mismatch in optical illumination conditions (particularly angular) between calibration and use. These will have caused the following types of error:

- A systematic radiometric error in the SRF. Any error that applies equally (in a relative sense) to all wavelengths will effectively "cancel out" as the SRF used is the normalised SRF.
- A random radiometric error in the SRF. The effect of random noise in the SRF estimate that is random from one discrete wavelength value to the next, will be minimised through the spectral integration, if enough discrete values are combined in that integration.
- Any error that affects the width of the SRF and/or which is asymmetrical across the SRF (for example faster degradation at shorter wavelengths than longer wavelengths) will be significant
- Any systematic bias of the wavelength scale (a shift to shorter or longer wavelengths) will be significant.

Appendix A.2 discusses some analysis with the spectral response function. Further work is needed to understand the implication for brightness temperature and whether an erroneous SRF will partially cancel out for some spectral bands where the scenes have a similar spectral shape to the IWCT. A dedicated document focussing on SRF shifts and associated uncertainties is under preparation.

The only error term considered in an effects table is a systematic wavelength shift. There is no correlation in the shift between channels, but the shift is considered identical for all measurements. It is therefore fully systematic, although the sensitivity coefficient will depend on local conditions.

Note that this table only considers the effect of the SRF spectral shift on the calibration. There is an additional effect when radiances are converted to brightness temperatures for all Earth scenes, but this is not yet included in the measurement equation.

Table 4 Effects tables for the SRF, considering a spectral shift

Table descriptor		
Name of effect		Spectral response function wavelength shift
Affected term in measurement function		$\xi(\lambda) \equiv \xi(\lambda + \delta_\lambda)$
Instruments in the series affected		All
Correlation type and form	**Pixel-to-pixel [pixels]**	Rectangular_absolute
	from scanline to scanline [scanlines]	Rectangular_absolute
	between images [images]	Rectangular_absolute
	Between orbits [orbit]	Rectangular_absolute
	Over time [time]	Rectangular_absolute
	Pixel-to-pixel [pixels]	$\left[-\infty, +\infty\right]$

Correlation scale	from scanline to scanline [scanlines]	$[-\infty, +\infty]$
	between images [images]	$[-\infty, +\infty]$
	Between orbits [orbit]	$[-\infty, +\infty]$
	Over time [time]	$[-\infty, +\infty]$
Channels/bands	List of channels / bands affected	All
	Error correlation coefficient matrix	Identity Matrix (no correlation)
Uncertainty	PDF shape	Gaussian
	units	μm
	magnitude	Provided as a single value based on sensitivity analysis
Sensitivity coefficient		See Eq 4-4 and Eq 4-8

Here the sensitivity coefficient is $\dfrac{\partial L_{\mathrm{E}}}{\partial \delta_\lambda}$. We will ignore the SRF in the self-emission radiances for simplicity,

so

$$\frac{\partial L_{\mathrm{E}}}{\partial \delta_\lambda} = \frac{\partial L_{\mathrm{E}}}{\partial \alpha}\frac{\partial \alpha}{\partial \delta_\lambda} = \left(C_{\mathrm{E}} - \bar{C}_{\mathrm{S}}\right)\frac{\partial \alpha}{\partial \delta_\lambda} \ .$$

$$\frac{\partial \alpha}{\partial \delta_\lambda} = \frac{\partial \alpha}{\partial \tilde{L}_{\mathrm{IWCT}}}\frac{\partial \tilde{L}_{\mathrm{IWCT}}}{\partial \delta_\lambda} = \frac{-1}{\bar{C}_{\mathrm{IWCT}} - \bar{C}_{\mathrm{S}}}\frac{\partial \tilde{L}_{\mathrm{IWCT}}}{\partial \delta_\lambda}$$

Eq 4-4

To understand $\dfrac{\partial \tilde{L}_{\mathrm{IWCT}}}{\partial \delta_\lambda}$, we need to write the integral in Eq 3-5 as the summation that is actually used:

$$\tilde{L}_{\mathrm{IWCT}} = \sum_i \left(\left(\varepsilon_{ch} + a_2\right)L_{\mathrm{BB}}\left(\lambda_i, T_{\mathrm{IWCT}}\right) + \left(1 - \varepsilon_{ch} - a_2\right)L_{\mathrm{refl}}\left(\lambda_i\right)\right)\xi_{ch}\left(\lambda_i\right)\ell_i + 0.$$

Eq 4-5

Here, ℓ_i is the multiplier used in the trapezium rule to represent step size. If we consider the sensitivity of this summation to an error in wavelength of the SRF, we get

$$\frac{\partial \tilde{L}_{\mathrm{IWCT}}}{\partial \lambda_i} = \sum_i \left(\left(\varepsilon_{ch} + a_2\right)L_{\mathrm{BB}}\left(\lambda_i, T_{\mathrm{IWCT}}\right) + \left(1 - \varepsilon_{ch} - a_2\right)L_{\mathrm{refl}}\left(\lambda_i\right)\right)\ell_i \frac{\partial \xi_{ch}\left(\lambda_i\right)}{\partial \lambda}$$

Eq 4-6

Now, if the wavelength error is random, we would add the sum of the squares because each λ_i would have a different error. But here we have a systematic wavelength error δ_λ. Therefore it is this whole expression that is squared, that is the uncertainty associated with $\tilde{L}_{\mathrm{IWCT}}$ due to a systematic wavelength error is

$$u^2\left(\tilde{L}_{\mathrm{IWCT}}\right)\Big|_{\delta_\lambda} = \left[\sum_i \left(\left(\varepsilon_{ch} + a_2\right)L_{\mathrm{BB}}\left(\lambda_i, T_{\mathrm{IWCT}}\right) + \left(1 - \varepsilon_{ch} - a_2\right)L_{\mathrm{refl}}\left(\lambda_i\right)\right)\ell_i \frac{\partial \xi_{ch}\left(\lambda_i\right)}{\partial \lambda}\right]^2 u^2\left(\delta_\lambda\right) \quad \text{*Eq 4-7*}$$

And thus we can write

$$\frac{\partial \tilde{L}_{\text{IWCT}}}{\partial \delta_\lambda} = \left[\sum_i \left(\left(\varepsilon_{ch} + a_2 \right) L_{\text{BB}} \left(\lambda_i, T_{\text{IWCT}} \right) + \left(1 - \varepsilon_{ch} - a_2 \right) L_{\text{refl}} \left(\lambda_i \right) \right) \ell_i \frac{\partial \xi_{ch} \left(\lambda_i \right)}{\partial \lambda} \right] \qquad Eq\ 4\text{-}8$$

The derivative of the SRF with respect to wavelength will be best determined numerically.

4.3   IWCT Radiance effects

The IWCT radiance is calculated from Eq 4-5 assuming that the IWCT is a greybody with an emissivity $\varepsilon_{ch} + a_2$ for a specific channel, and a temperature given by

$$T_{\text{IWCT}} = \left(\frac{1}{N} \sum_i T_{\text{PRT},i} \right) + 0 \qquad Eq\ 4\text{-}9$$

As the simple mean of temperatures $T_{\text{PRT},i}$ measured by the N PRTs. The +0 here represents the assumption that the mean PRT signal is equal to the temperature of the IWCT averaged over the field of view of the radiometer.

As well as the SRF wavelength shift, the band-integrated radiance of the IWCT is affected by the following components:

- Noise in individual PRT counts
- Systematic calibration bias of the PRTs
- Emissivity of the IWCT
- Representativeness of the mean of the PRTs to the observed IWCT temperature
- Earthshine onto the IWCT

As these have different correlation structures they must be considered separately.

The noise in the PRT counts is a structured random effect, it is random from one measurement to the next, but since the determined IWCT radiance is used for all pixels in all scanlines within the calibration cycle of HIRS, this effect is constant for that calibration cycle. Because the noise in the individual PRTs are independent from one another, we can determine the uncertainty associated with noise in the mean PRT signal, which will be the noise in any individual PRT divided by $\sqrt{N}$. It is that noise that is included in the table. Here the noise is in counts. This is corrected to temperature with a sensitivity coefficient of temperature to counts.

The systematic calibration bias of the PRTs comes from the accuracy of the original PRT calibration, from any post-calibration drift and from the offset of the PRTs from the front surface of the IWCT. This is a fully systematic uncertainty component. The uncertainty is expressed in kelvin. Note that we do not consider uncertainties in the calibration coefficients for the fifth order polynomial used to convert counts to

temperature. This is because those coefficients will be correlated and were determined from a temperature calibration and therefore it is better to think of uncertainties in terms of temperature[6].

Uncertainty in the emissivity of the IWCT is not considered. This is because the a_2 term, determined during harmonisation, is designed to correct any emissivity error.

The mean PRT measurement will not be representative of the observed temperature by the HIRS instrument if there are non-linear thermal gradients across the IWCT. To estimate the possible extent of this, the maximum difference between any one PRT and the mean is considered the extent of representativeness and this is considered a rectangular distribution (i.e. the standard uncertainty is the maximum observed offset divided by the square root of three). Later it may be possible to do a more detailed study by fitting a plane to some of the PRTs and looking at the difference of the others to that plane.

Earthshine creates the reflected term, L_{refl} in Eq 4-5. This effect has not yet been studied in detail. If it is significant it will be corrected for. If it is corrected for, then the uncertainty is that associated with the correction. For now we will consider this to be a structured random effect with the same correlation structure as the other IWCT components, but this may change if more information becomes available from the study.

All of these effects, except Earthshine are correlated between channels because the same IWCT temperature is assumed for all channel calibrations.

Table 5 Effects tables for the IWCT band-integrated radiance

Table descriptor					
Name of effect		PRT count noise	PRT bias	PRT representativeness	Earthshine
Affected term in measurement function		$\tilde{L}_{IWCT}$	$\tilde{L}_{IWCT}$	$\tilde{L}_{IWCT}$	$\tilde{L}_{IWCT}$
Instruments in the series affected		All	All	All	TBC
Correlation type and form	**Pixel-to-pixel [pixels]**	Rectangular Absolute	Rectangular Absolute	Rectangular Absolute	Rectangular Absolute
	from scanline to scanline [scanlines]	Stepped triangle absolute	Rectangular Absolute	Bell-shaped	Rectangular absolute
	between images [images]	N/A	N/A	N/A	N/A
	Between orbits [orbit]	Random	Rectangular Absolute	Bell-shaped	Rectangular absolute
	Over time [time]	Random	Rectangular Absolute	Random	Rectangular absolute
Correlation scale	**Pixel-to-pixel [pixels]**	$[-\infty, +\infty]$	$[-\infty, +\infty]$	$[-\infty, +\infty]$	$[-\infty, +\infty]$

---

[6] For TIROS-N and NOAA-6,-7,-8 we do not have the coefficients at all.

	from scanline to scanline [scanlines]	Provided for each scanline to define the stepped rectangular absolute Window is (a+b+1) scanlines, rolling average over n windows [-a,+b, n]	Provided for each scanline to define the stepped rectangular absolute	A function will be provided but we expect the correlation length to be in the order of some hundreds of scanlines. TBC.	$[-\infty, +\infty]$
	between images [images]	N/A	N/A	N/A	N/A
	Between orbits [orbit]	[0]	[0]	TBC	$[-\infty, +\infty]$
	Over time [time]	[0]	[0]	[0]	$[-\infty, +\infty]$
Channels/ bands	**List of channels / bands affected**	All	All	All	TBC
	Correlation coefficient matrix	Matrix of 1s everywhere	Matrix of 1s everywhere	Matrix of 1s everywhere	Identity matrix (diagonal only)
Uncertainty	**PDF shape**	Gaussian	Gaussian	Rectangular	??
	units	Counts (or kelvin)	kelvin	kelvin	mW m^{-2} sr^{-1} µm
	magnitude	Provided per calibration cycle. Note this is uncertainty for the mean	0.1 K everywhere	Provided per calibration cycle. Note – maximum divided by $\sqrt{3}$	Provided per calibration cycle.
Sensitivity coefficient		$\dfrac{\partial L_\mathrm{E}}{\partial \bar{C}_\mathrm{PRT}}$,	$\dfrac{\partial L_\mathrm{E}}{\partial T_\mathrm{IWCT}}$	$\dfrac{\partial L_\mathrm{E}}{\partial T_\mathrm{IWCT}}$	$\dfrac{\partial L_\mathrm{E}}{\partial L_\mathrm{refl}}$

All of these sensitivity coefficients will share the same initial step

$$\frac{\partial L_\mathrm{E}}{\partial \tilde{L}_\mathrm{IWCT}} = \frac{\partial L_\mathrm{E}}{\partial \alpha}\frac{\partial \alpha}{\partial \tilde{L}_\mathrm{IWCT}} = \frac{-\left(C_\mathrm{E} - \bar{C}_\mathrm{S}\right)}{\bar{C}_\mathrm{IWCT} - \bar{C}_\mathrm{S}} \quad . \qquad\qquad \textit{Eq 4-10}$$

The first three also need

$$\frac{\partial \tilde{L}_{\text{IWCT}}}{\partial T_{\text{IWCT}}} = \sum \frac{\partial \tilde{L}_{\text{IWCT}}}{\partial L_{\text{BB}}(\lambda_i)} \frac{\partial L_{\text{BB}}(\lambda_i)}{\partial T_{\text{IWCT}}} \quad , \qquad \textit{Eq 4-11}$$

where

$$\frac{\partial \tilde{L}_{\text{IWCT}}}{\partial L_{\text{BB}}(\lambda_i)} = \left(\varepsilon_{ch} + a_2\right)\xi_{ch}(\lambda_i)\ell_i. \qquad \textit{Eq 4-12}$$

$$\frac{\partial L_{\text{BB}}}{\partial T_{\text{IWCT}}} = \frac{L_{\text{BB}}(\lambda,T)hc}{\lambda k_{\text{B}} T_{\text{IWCT}}^2 \left(1 - \exp\left[-hc/(\lambda k_{\text{B}} T_{\text{IWCT}})\right]\right)} \qquad \textit{Eq 4-13}$$

The sensitivity coefficient for Earth radiance to the uncertainty in the average PRT counts has the longest required chain rule

$$\frac{\partial L_{\text{E}}}{\partial \bar{C}_{\text{PRT}}} = \frac{\partial L_{\text{E}}}{\partial \alpha} \frac{\partial \alpha}{\partial \tilde{L}_{\text{IWCT}}} \frac{\partial \tilde{L}_{\text{IWCT}}}{\partial T_{\text{IWCT}}} \frac{\partial T_{\text{IWCT}}}{\partial \bar{C}_{\text{PRT}}} \quad . \qquad \textit{Eq 4-14.}$$

To determine $\dfrac{\partial T_{\text{IWCT}}}{\partial \bar{C}_{\text{PRT}}}$ we need to consider the calibration equations for the PRTs. In practice we will do this outside the effects table and provide an uncertainty in kelvin in the effects table.

4.4   Self-emission effects

The HIRS optical train and detector are not cooled. Therefore, any measurement is contaminated by large amounts of self-emission, such as indicated in the measurement function. If this self-emission were constant, it would be cancelled out due to calibration. Self-emission does vary as a function of instrument temperature (as one would expect), in particular on an orbital timescale. Self-emission also leads to variations in the gain, because of the non-linear response of the detector. Although this is corrected for by the calibration, those calibrations are too infrequent and a model is needed to estimate self-emission between the calibrations.

To estimate self-emission perfectly, one would need to know the temperature, emissivity, and solid angle, for all components directly visible by the detector. One would additionally need to know how any other radiation is reflected onto the detector. This would require substantially more information both before launch and in-orbit than is actually being measured. Therefore, self-emission is approximated as shown in Eq. 3-6.

HIRS reports temperatures for the following components:

- Patch
- Filter wheel motor
- Scan motor
- Internal warm calibration target
- Internal cold calibration target (HIRS/2 only)
- Primary telescope
- Secondary telescope
- Tertiary telescope (HIRS/4 only)

- Electronics
- Baseplate
- Scan mirror

Although this is not enough to make a complete model of self-emission, it is likely enough to make a sufficiently approximate model. This model is being developed by studying what components or combination thereof most accurately predict the Δ in self-emission between calibration cycles. Figure 8 gives an example, but the details depend on the instrument, but can also vary on short and long time scales throughout an instrument's lifetime. The thermal environment within an instrument can change if HIRS is switched off and on again, or if another instrument on the same satellite is switched on and off again, and certainly as the orbit drifts over time. Therefore, coefficients in such a model need to be continuously updated, and uncertainties need to be continuously estimated.

In the model, we update the coefficients every 6 hours using a 24-hour window.

- Within a scanline, both coefficients and instrument temperatures are identical; each scanline has a single self-emission correction estimate, so the errors are systematic with a rectangular absolute correlation form.
- Within each 6-hour cycle using a 24 hour window, the coefficients are a constant error source, but temperatures vary per scanline. The next 6-hour cycle shares (24-6)/24*100 %=75 % of training data (temperatures and offsets), so there is an error correlation between the coefficients of nearby cycles. This is described by stepped triangle absolute.
- Between orbits and longer times, a similar thermal environment on the spacecraft is expected to yield a similar error. That means the correlation between orbits is rectangular absolute, on time scales of up to several days or weeks. There may also be a seasonal cycle, described here by repeating bell shapes.

Table 6 Effects tables for the self-emission

Table descriptor		
Name of effect	Self-emission model errors – Earth view	
Affected term in measurement function	$L_{\text{self,E}}$	
Instruments in the series affected	All	
Correlation type and form	**Pixel-to-pixel [pixels]**	Rectangular_absolute
	from scanline to scanline [scanlines]	Stepped triangle absolute
	between images [images]	n/a
	Between orbits [orbit]	Rectangular absolute
	Over time [time]	Repeating bell shapes
Correlation scale	**Pixel-to-pixel [pixels]**	$\left[-\infty, +\infty\right]$
	from scanline to scanline [scanlines]	provided as [-a, b, n], where a+b=~3860, n=4
	between images [images]	n/a
	Between orbits [orbit]	TBC – needs more study

	Over time [time]	TBC – needs more study
Channels/bands	**List of channels / bands affected**	All
	Error correlation coefficient matrix	Matrix of all 1s
Uncertainty	**PDF shape**	Gaussian
	units	mW m^{-2} sr^{-1} cm
	magnitude	Provided as a single value based on modelling
Sensitivity coefficient		Eq 4-15

Where the sensitivity coefficients are given by

$$\frac{\partial L_{\text{E}}}{\partial L_{\text{self,E}}} = -1.$$

<div align="right">*Eq 4-15*</div>

$$\frac{\partial L_{\text{E}}}{\partial L_{\text{self,S}}} = \frac{\left(C_{\text{E}} - \bar{C}_{\text{S}}\right)}{\bar{C}_{\text{IWCT}} - \bar{C}_{\text{S}}} - 1.$$

<div align="right">*Eq 4-16*</div>

$$\frac{\partial L_{\text{E}}}{\partial L_{\text{self,S}}} = \frac{-\left(C_{\text{E}} - \bar{C}_{\text{S}}\right)}{\bar{C}_{\text{IWCT}} - \bar{C}_{\text{S}}} + 1.$$

<div align="right">*Eq 4-17*</div>

4.5 Model assumptions

The +0 term in the main equation, Eq 3-3, considers the following effects:

- Wrongness of the quadratic approximation to non-linearity. Although we use a quadratic to model the non-linearity of the detectors, the physics of the detector would lead one to expect a different behaviour. See also the AVHRR section of D2.2, appendix A5; the impact for HIRS will be smaller than that for AVHRR due to the spectrally narrower filters.
- Undesired electronics effects, not otherwise covered. This covers a number of different behaviours observed in the data but where the physical origins are poorly understood. In the effects table, the correlation types have all been listed as "rectangular absolute", but this is still to be confirmed. Until this is confirmed, "rectangular absolute" is the most conservative assumption.

Table descriptor			
Name of effect		Wrongness of quadratic approximation	Undesired electronics effects
Affected term in measurement function		0	0
Instruments in the series affected		All	All
Correlation type and form	**Pixel-to-pixel [pixels]**	Rectangular Absolute	Rectangular Absolute
	from scanline to scanline [scanlines]	Rectangular Absolute	Rectangular Absolute

	between images [images]	N/A	N/A
	Between orbits [orbit]	Rectangular Absolute	Rectangular Absolute
	Over time [time]	Rectangular Absolute	Rectangular Absolute
Correlation scale	Pixel-to-pixel [pixels]	$[-\infty, +\infty]$	$[-\infty, +\infty]$
	from scanline to scanline [scanlines]	$[-\infty, +\infty]$	$[-\infty, +\infty]$
	between images [images]	N/A	N/A
	Between orbits [orbit]	$[-\infty, +\infty]$	$[-\infty, +\infty]$
	Over time [time]	$[-\infty, +\infty]$	$[-\infty, +\infty]$
Channels/ bands	List of channels / bands affected	All	All
	Correlation coefficient matrix	TBC, but likely a block matrix per detector	TBC, may be a matrix of ones or a block matrix per detector
Uncertainty	PDF shape	Gaussian	Gaussian
	units	mW m^{-2} sr^{-1} cm	mW m^{-2} sr^{-1} cm
	magnitude	TBC	TBC
Sensitivity coefficient		1	1

5 Harmonisation

Harmonisation is described separately, so only a brief overview is considered here. The harmonisation coefficients a_1, a_2, a_3 represent the non-linearity of the instrument, the bias due to straylight differences between the calibration and observation views and an emissivity correction respectively. The harmonisation process will determine these parameters, and a covariance matrix for the parameters. To propagate these uncertainties through to the uncertainty associated with the Earth radiance we need the sensitivity coefficients:

$$\frac{\partial L_{\mathrm{E}}}{\partial a_1} = C_{\mathrm{E}}^2 - C_{\mathrm{E}} C_{\mathrm{IWCT}} - C_{\mathrm{E}} C_{\mathrm{S}} + C_{\mathrm{IWCT}} C_{\mathrm{S}} \qquad \text{Eq 5-1}$$

$$\frac{\partial L_{\mathrm{E}}}{\partial a_2} = \frac{\partial L_{E}}{\partial L_{\mathrm{IWCT}}} \frac{\partial L_{\mathrm{IWCT}}}{\partial a_2}$$
$$\frac{\partial L_{\mathrm{IWCT}}}{\partial a_2} = L_{\mathrm{BB}} - L_{\mathrm{refl}} \qquad \text{Eq 5-2}$$

$$\frac{\partial L_{\mathrm{E}}}{\partial a_3} = 1 \qquad\qquad Eq\ 5\text{-}3$$

A   Appendix on detailed information about uncertainty components

A.1   Noise and cross talk, correlations observed

The noise for space counts, and IWCT counts are all determined from repeated observations of the space view and the IWCT. Visualising only the anomalies, the space views for three different channels may look somewhat like in Figure 2.
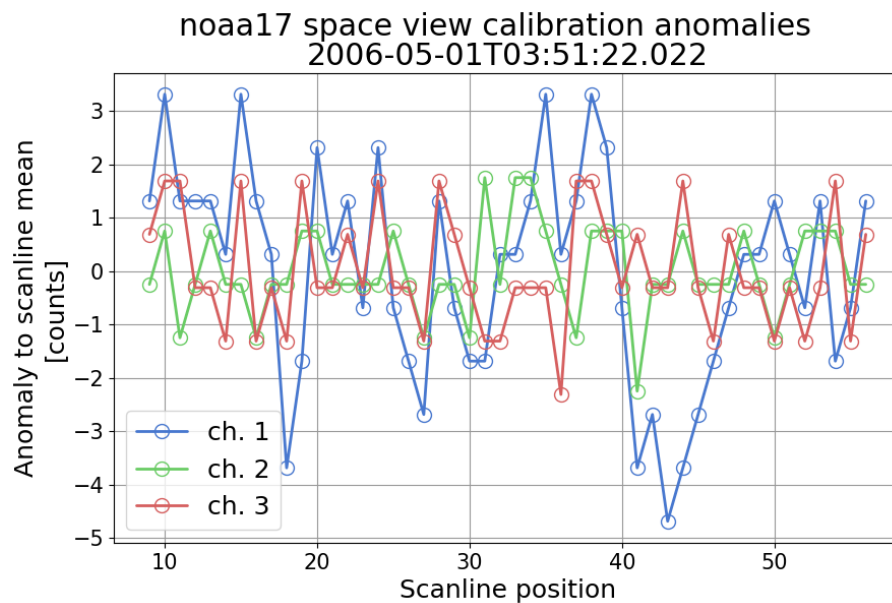

Figure 2: space view calibration anomalies

The uncertainty in the Earth counts is determined as the Allan deviation (see D2-2a) for the 48 positions. The uncertainty for the space counts is the same, but divided by $\sqrt{48}$. The uncertainty on the IWCT is determined from the (similar-looking) series of IWCT views. This uncertainty is primarily due to noise and may vary significantly over the lifetime of an instrument, as shown in Figure 3 for NOAA-16 channel 5. Other channels and HIRS on other satellites also show noise variability on short and long timescales.
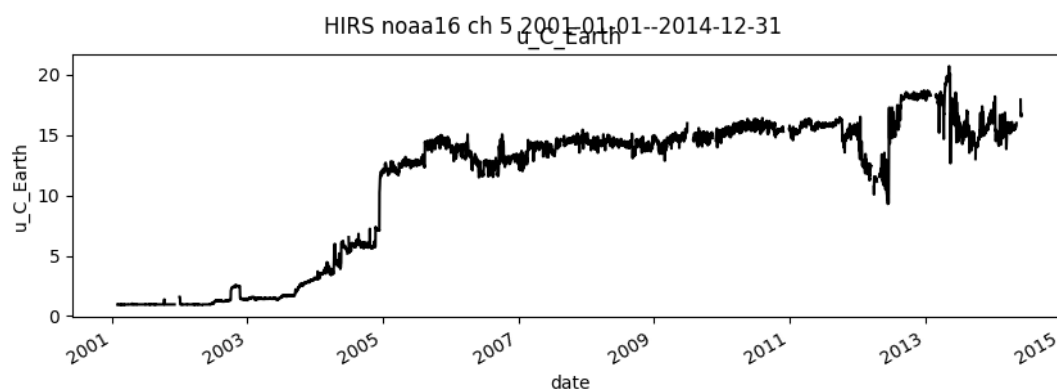
Figure 3: Noise in Earth counts over the lifetime of NOAA-16 HIRS

In some cases, there is an unexpected correlation between the anomalies, such as shown in Figure 4, which shows two phenomena. Firstly, there is clearly a correlation between the "noise" in the different channels. Secondly, there is a period signal causing correlation between the "noise" of subsequent observations.
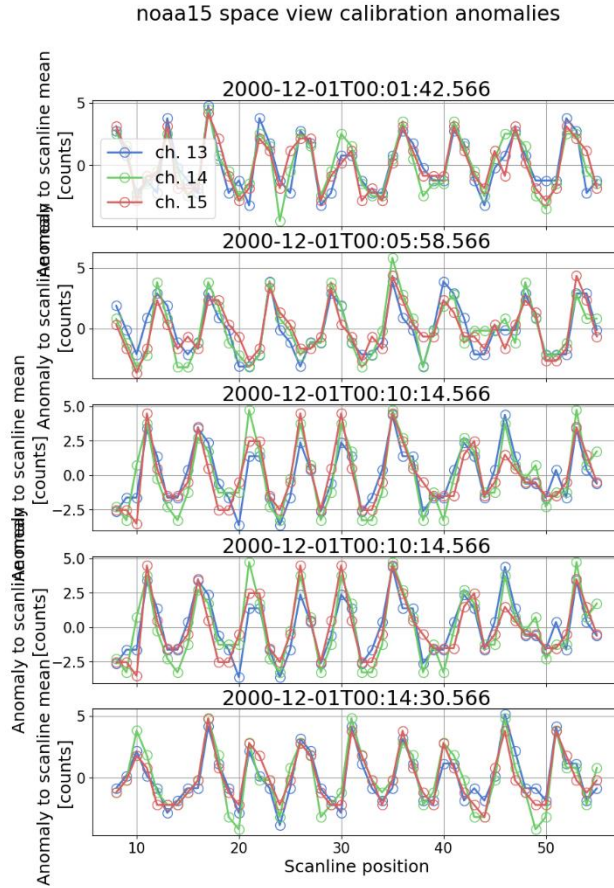
Figure 4: like Figure 2, but for some cases with extreme correlations between channels.

To estimate noise correlations between channels, we calculate the mean $\left\langle C_m \right\rangle_{\mathrm{ch}}$ for each calibration cycle, where m relates to space or IWCT views and ch to a channel. For any calibration position n (e.g. $n = 20$) we calculate the anomaly,

$$\tilde{C}_{n,\mathrm{ch}} = C_{n,\mathrm{ch}} - \left\langle C_m \right\rangle_{\mathrm{ch}} \; .$$

<div align="right">*Eq 5-4.*</div>

and calculate the correlation matrix between those channels. Values for those correlations can be either positive or negative, are usually nonzero even between different detectors, vary between instruments and as an instrument ages. Figure 5 shows an example of such a correlation matrix.

The spectrum / colour of noise is still to be investigated.
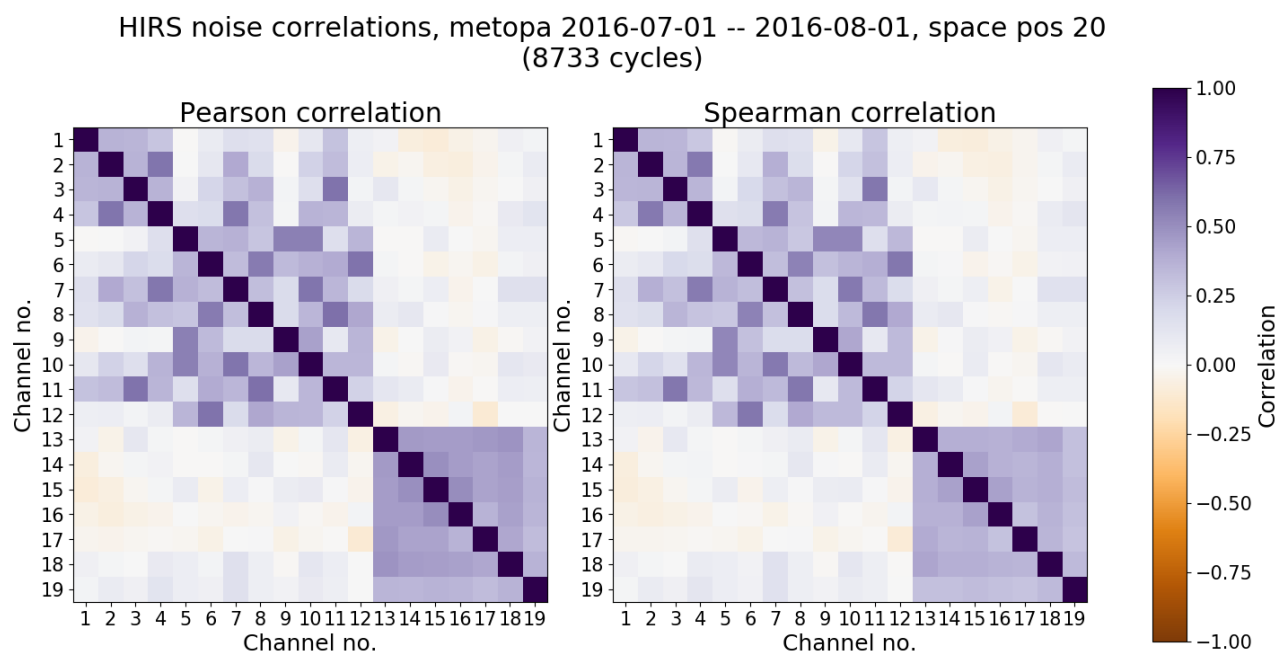
Figure 5: Correlation matrix between MetOp-A channels. The different panels show the Pearson and Spearman correlation, respectively, in order to confirm the correlation is not caused by outliers.

A.2 Spectral response function biases

The recovery of spectral shifts in SRF will have an error. A dedicated document (PD4.4) is in preparation and will describe in detail how the spectral shifts are recovered, and how the uncertainties are estimated. The contents of this appendix are an excerpt from PD4.4.

A.2.1 Prior work

Chen, Cao and Menzel (2013) describe a homogenisation process of HIRS channels 4–7 on satellites NOAA-9–19 and MetOp-A. They use Simultaneous Nadir Observations (SNOs) involving both HIRS and the Infrared Atmospheric Sounding Interferometer (IASI) to find the SRF shift that minimises differences between instances of HIRS. They find shifts of up to 3 cm−1 for NOAA-14 channel 5, which at the centre wavelength of 14 μm corresponds to a wavelength shift of 58 nm. However, they do not include other channels or earlier satellites and do not consider an uncertainty analysis[7] .

Chen and Cao (2012) compare HIRS channels 4–8 with IASI-simulated HIRS on MetOp. They consider a "blackbody bias" by comparing Earth views with the same temperature as the Internal Warm Calibration Target (IWCT), then compensate for this bias before proceeding with estimating SRF errors and nonlinearities.

Cao, Goldberg and Wang (2009) use IASI to simulate radiances for 14 HIRS instruments from Television InfraRed Observation Satellite (TIROS)-N through MetOp-A. They look at the radiance ratio between pairs of HIRS for a selection of IASI orbits, and show that this can explain observed differences from SNOs, in particular for NOAA-14/-15 channel 4.

---

[7] Those are included in RTTOV — according to https://nwpsaf.eu/downloads/rtcoef_rttov11/ir_srf/ rtcoef_noaa_15_hirs-shifted_srf.html HIRS spectral shifts are provided by ruiyue.chen@noaa.gov.

23

Cao et al. (2005) study the differences between NOAA-15, -16, and -17 using SNOs. They find seasonally dependent differences in the sounding channels, and speculate this can be best explained by SRF differences.

Other relevant prior work includes studies by Shi, Bates and Cao (2008), Shi and Bates (2011) and Shi (2013). None of the previous studies estimate uncertainties based on metrological traceability.

A.2.2 HIRS SRFs

SRFs have been measured before launch with varying degrees of accuracy. For the present study, we obtained measured SRFs from NOAA National Environmental Satellite, Data, and Information Service (NESDIS) The Center for Satellite Applications and Research (STAR) National Calibration Center (NCC) at https://cs.star.nesdis.noaa.gov/NCC/SRFHIRS.

Ideally, SRFs for the same channel would be identical between different instances of HIRS, but in reality they differ between instruments and possibly during the lifetime of a particular instrument instance. Apart from two instances where a channel was moved on purpose, most differences between the same channel on different instances of HIRS are not by design.

IASI is a hyperspectral radiometer measuring infrared radiation in 8461 channels in a range of 3.62 to 15.50 μm. It flies on-board the EUMETSAT MetOp satellite series, starting with MetOp-A in 2006. This gives a period of more than 10 years during which IASI and HIRS co-exist. IASI is useful reference for HIRS, both for the study of SRFs and in other contexts, such as harmonisation. We can use IASI to simulate HIRS channel radiances with arbitrary SRFs.

Figure 6 illustrates a fragment of the spectrum as measured by IASI on MetOp-A, with superimposed the SRFs as measured before launch, for all satellites. The figure illustrates that measured SRFs differ. In case of channel 4, that alone accounts for BT differences of up to 5K. In channel 15 (not shown here) those differences regularly exceed 10 K.
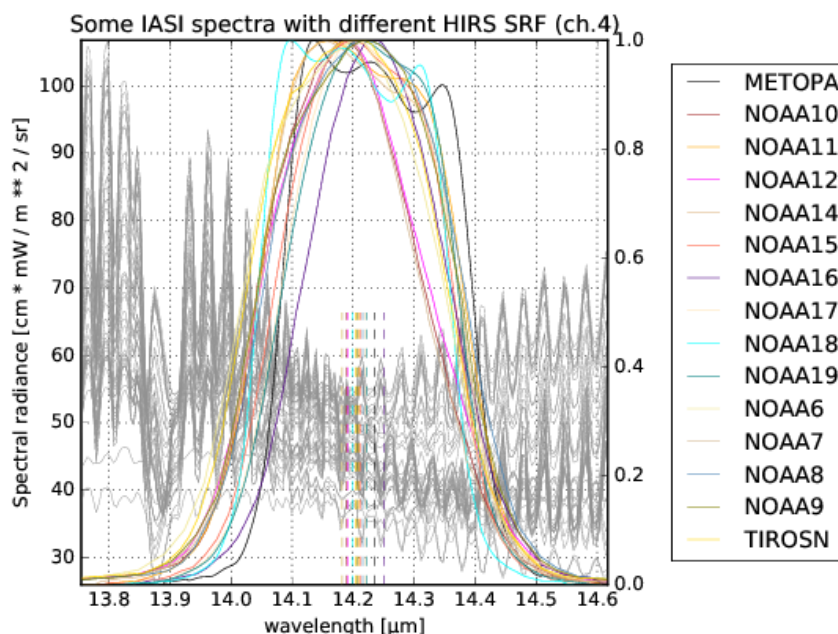

Figure 6: Fragment of global random selection of IASI spectra with measured SRF for channel 4 for all HIRS-carrying satellites. The dashed vertical lines indicate the centroid for each satellite.

A.2.3 SRF error propagation

Spectral shift errors in the SRF propagate through to errors in the calibrated radiance in several ways:

- It will cause a systematic error in calibrated IWCT radiance. This then propagates through to all radiances calibrated with this IWCT.
- It introduces an error when converting from radiance units to BT units. Although this is not covered in the measurement diagram, which remains in radiance space, it is relevant for most users because most users use brightness temperatures in units of K.
- It introduces an error in the interpretation of the radiance or brightness temperature. Even if a radiance is otherwise correct within its uncertainty bounds, an erroneous SRF will lead to analysis errors for some users, for example, when using radiative transfer simulations, as commonly done in retrieval development.

A.2.4 SRF shift recovery and uncertainty

Using a set of channels on satellite k + 1, we predict the radiance for a single channel on satellite k, assuming either the measured or a shifted SRF. When using collocations, this prediction can be compared against the real measurement for satellite k, thus determining whether either the measured or shifted SRF is consistent with radiance differences.

By imposing a shift in simulated data, then applying our recovery method, we can determine statistically how well we are able to recover the shift. If we additionally add simulated noise in the recovery method, we can determine how sensitive the recovery is to noise in the reference radiances.

Figure 7 shows the results of a simulation exercise, where a shift was imposed, then a recovery was attempted. The colours indicate the magnitude of the reference shift that was attempted to be recovered. Different dots for the same shift refer to different noise levels. The figure shows how an error in the SRF recovery propagates to a systematic error in calibrated radiances. Details can be found in PD4.4.
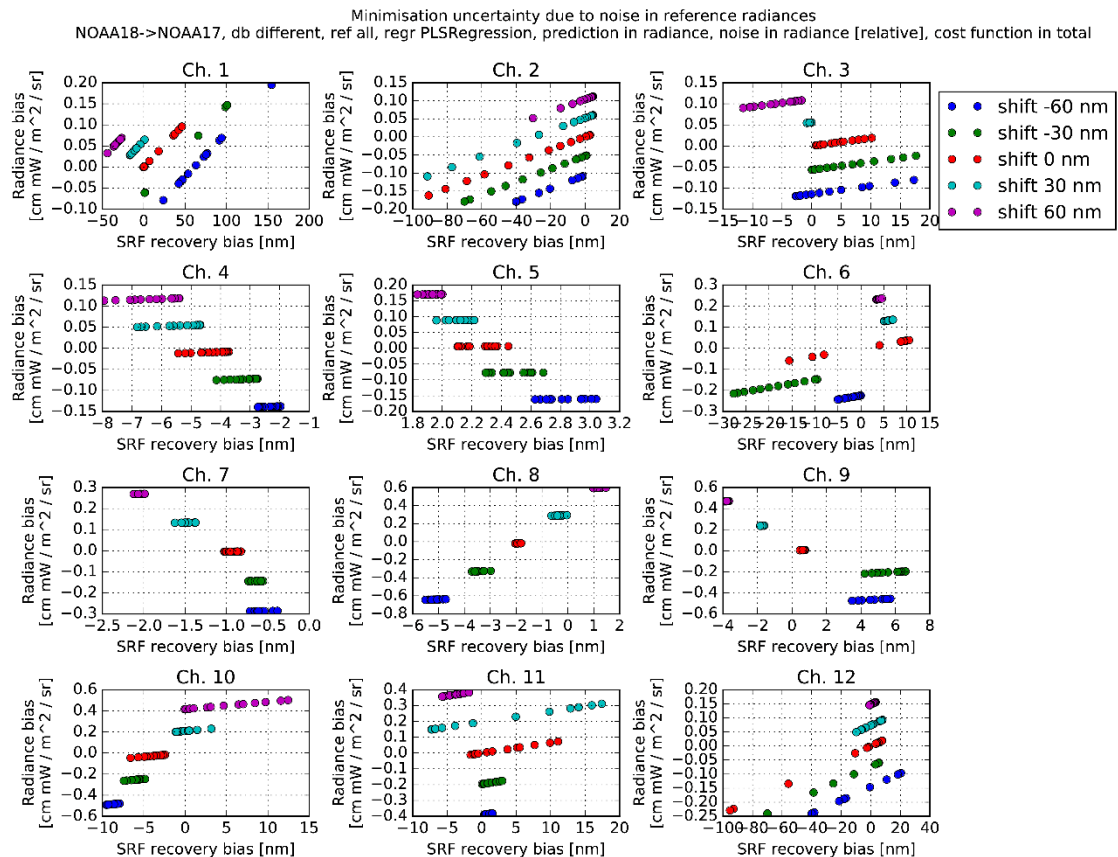
Figure 7 propagation of SRF recovery bias to radiance bias

The SRF recovery study still needs further work and needs to be integrated into the harmonisation. For the current version of the pre-beta easy FCDR, pre-launch SRFs are used and their uncertainty is not informed by the aforementioned study, but set to more or less arbitrary values of between 1 nm and 15 nm depending on the variation in SRFs between spacecraft for a particular channel.

A.3 Self-emission

The HIRS detector is not cooled and HIRS experiences significant self-emission. With frequent calibration, this would not be problematic, but calibration is only performed every 40 scanlines (256 seconds) and the thermal environment of the spacecraft is changing. This necessitates the development of a model for self-emission.

Figure 8 illustrates the difference between HIRS and IASI-simulated HIRS as a function of the number of scanlines since the last calibration cycle, when self-emission is ignored. The figure shows that in cases where the satellite is heating up between scanlines, ignoring changes in self-emission leads to a systematic error of 0.6 mW m^{-2} sr^{-1} cm. In cases where it is cooling down, the systematic error would be -0.4 mW m^{-2} sr^{-1} cm. That error is correctable with a self-emission model.
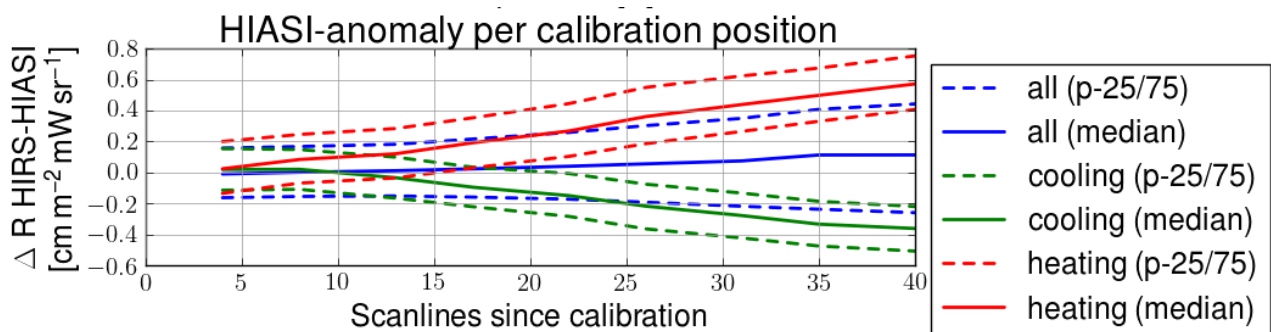
Figure 8: Difference between HIRS and IASI as a function of the number of scanlines since calibration, if self-emission is ignored, for all cases, cooling cases, or heating cases.

Existing approaches to self-emission are simple and lack an uncertainty estimate. Chang and Cao (2014) present a self-emission model with parameters trained on a limited period, but do not account for the fact that those parameters may change when the thermal environment of the instrument changes, and do not estimate any uncertainties associated with it.

Our self-emission model is presented in Eq 3-8. As described, we update the self-emission model every 6 hours, determining the parameters using linear regression. Within this 6 hour window, we use half the space views as training data and half the space views as testing data. Currently, the uncertainty estimate is a single number for this window, determined by the room mean square error of the reference self-emission change minus the estimated self-emission change.